String Tests of 3S1P Configurations for Electric Energy Storage Applications

Prepared for the

U.S. Department of Energy
Office of Electricity Delivery and Energy Reliability

Under Cooperative Agreement No. DE-FC26-06NT42847
Hawai‘i Distributed Energy Resource Technologies for Energy Security

Subtask 11.2 Deliverable 2
Report on Results of Storage Tests

Prepared by

Hawai‘i Natural Energy Institute
School of Ocean and Earth Science and Technology
University of Hawai‘i

December 2012

Acknowledgement: This material is based upon work supported by the United States Department of Energy under Cooperative Agreement Number DE-FC-06NT42847.

String Tests of 3S1P Configurations for Electric Energy Storage Applications

Matthieu Dubarry and Bor Yann Liaw
Hawaii Natural Energy Institute, SOEST, University of Hawaii
1680 East-West Road, POST 109, Honolulu, HI 96822
(808) 956-2339, bliaw@hawaii.edu

Table of Contents

1. INTRODUCTION

As the scale of energy storage applications for electric grids increase, the number of cells used in these battery systems also increase. Thus, the reliability and safety of large battery systems hinge on effective management and control of these systems. Besides the issues of cell consistency and the process to select cells for battery pack assembly that are critical to overall battery system performance, it is equally important to understand how the battery control and management strategy affects battery system performance. This project is designed to address the latter aspects, with some preliminary testing of battery string performance to guide our research.

Under funding from this grant, staff from HNEI conducted battery testing to investigate how control strategies applied to cells and strings impact system performance. Testing to determine the cell variability and performance were funded and reported under a separate grant [1]. The baseline performance of each cell was established in order to investigate these cells in multi-cell configurations.

For this project, a unique test protocol and analysis approach was developed in HNEI's electrochemical laboratory that can be used to study string performance issues beyond the conventional laboratory cell testing [1-4]. This approach comprises a sequence of test routines modified from those defined by the US Department of Energy in the US Advanced Battery Consortium (USABC) test manual and procedures. In order to reach a deeper understanding of the cell electrochemical behavior without adding too much time to the procedure we replaced the hybrid pulse power characterization (HPPC), electrochemical impedance spectroscopy (EIS), and constant power cycling steps by regular constant current cycling at different rates with extended rest time and residual capacity measurements. With this in-house analytical scheme, detailed cell performance parameters can be derived that help assess the feasibility of cell chemistry and design for certain stationary grid-tied applications.

To study multi-cell configurations and their performance issues, the basic configuration is a three-cell string typically noted in the industry as 3S1P. The 3S1P configuration provides the basis for quantitative analysis using a minimum number of cells while maintaining sufficient complexity in performance variability to support achieving the project objectives.

Under this task, three-cell (3S1P) strings, one from Altairnano and one from SAFT, are tested under RPT conditions (cycling at C/25, C/5, C/2, 1C, 2C and >2.5C rates with extended rest periods and residual capacity measurements) that are designed to show the impact of the three control strategies (string level, cell level, or (State of Charge (SOC) range) on string performance.

2. EXPERIMENTAL

2.1. Cell and Chemistry Selection

As stated, the two (2) families of cells were selected for this project and basic information covering cell characteristics is summarized herein (refer to Table 1) to provide useful background for discussion.

Six Altairnano nLTO cells (ALT cells) were purchased directly from the manufacturer for the project. The ALT cell design, with a rated capacity of 13 Ah, comprises nano-$Li_4Ti_5O_{12}$ (nLTO) as an active material in the negative electrode and $Li(Ni_xMn_yCo_z)O_2$ (NMC) in the positive electrode built in a prismatic pouch-shaped configuration. The specific composition of nLTO was not disclosed by the manufacturer (Altairnano). The nominal cell voltage is 2.2 V with a specific energy of 75 Wh/kg, as estimated from the nominal cell voltage, rated capacity, and nominal weight of the cell. The specific power was not disclosed by the vendor, nor could be estimated from the specification.

The second batch of cells consisted of four SAFT VL12V cells (SVL cells) that were made available to HNEI by SAFT. The cell design, with a rated capacity of 14 Ah, consists of a graphite anode and $Li_x(Ni_{0.8}Co_{0.15}Al_{0.05})O_2$ (NCA) cathode in a cylindrical shape. The nominal cell voltage is 3.6 V. The specific energy is74 Wh/kg and the specific power is 6 kW/kg in continuous operation.

Table 1 Specifications and characteristics of the cells selected for this string project

Cell Model	13Ah nLTO	VL12V
Vendor	Altairnano	SAFT
Form	Prismatic	Cylindrical
Chemistry PE	NMC	NCA
Chemistry NE	LTO	Graphite
Nominal Capacity	13 Ah	14 Ah
Nominal Voltage	2.2 V	3.6 V
Discharge cutoff voltage (V)	1.8	2.5
Charge cutoff voltage (V)	2.8	4.1
Specific Energy (Wh/kg)	75	74
Specific Power (kW/kg)	-	6

2.1.1. Baseline performance tests on single cells

To establish the baseline performance characteristics of a cell design and its chemistry, a reference performance test (RPT) is used to determine a single cell's properties. The RPT is typically conducted at room temperature using constant-current discharge (CCD) regimes with the following rates: C/25, C/5, C/2, 1C, 2C, and 3C. The charge regime uses the same rate as in the intended discharge regime to charge the cell (thus, a constant-current charge "CCC" regime) and then a constant-current trickle charge (CCTC) regime at C/25. The intent of the CCTC regimes is to determine the amount of charge return still available after the initial charge regime. This measurement also provides information about the state of charge (SOC) at the end of the initial charge regime. A rest period of 1-4 hours is also instituted between any test regimes under open-circuit condition to measure the rest cell voltage (RCV) to determine the SOC of the cell for further analysis. These procedures are already discussed in Refs [1-4], and supplemented by additional discussions in Refs [9-17], which outlined the entire process of cell evaluations including cell aging analysis and modeling.

All of the tests were performed at room temperature.

During testing of the SVL cells, the same schedule was used except the highest rate used for the test was limited to 2.5C, instead of 3C, due to a current limitation of HNEI's SVL test equipment. In addition to the RPT, 120 cycles of 3C cycle aging were applied to one ALT cell (cell #1) to extract the information regarding its initial stage of degradation as a preliminary result.

The initial conditioning and performance characterization tests of these cells during single cell testing was reported in a separate report [1] and summarized in Table 2. These single cell testing protocols comprise isothermal CCD regimes to determine the capacity of the cell under various rates, typically C/2 and C/5, to assess the capacity variations with rate. The dependence of capacity as a function of discharge rate is often called the rate capability. We have shown in our previous work [7, 10, and 13] that three parameters are critical to characterize the quality and variability of a batch of cells. Those parameters are the rate capability, the "capacity ration" (i.e. the mAh capacity per one percent of SOC, which is usually the cells maximum capacity), and the ohmic resistance. For the rate capability and the capacity ratio, any standard variation under 2% is considered acceptable in the industry to date, although less than 1% is desirable. For the ohmic resistance, a 10% standard deviation is considered acceptable as well with 5% being desirable.

As shown in Table 2, we recorded a rate capability variation of 0.85% for the ALT cells, a 0.6% capacity ration variation, and a 10 % ohmic resistance variation. For the SVL cell, the variation of rate capability, capacity ration, and resistance were 0.2%, 1.5%, and 5.7% respectively.

In summary, both batches of cells are sufficiently consistent to be used for multi-cell string testing with sufficient confidence that all cells will produce nearly identical results. Subsequently cell #1 of each batch was subjected to the baseline performance tests, as a control cell, and two of the remaining cells in the batch are arbitrarily selected for the 3S1P string tests.

2.1.2. Performance of 3S1P strings

Since the cell variability was so small (*cf* section 2.1.1) we introduced additional cell variations by design of experiments to study the impact of control strategies on system performance. The following protocols were used in the RPTs for the 3S1P strings:

(1) Each 3S1P string was tested with a 5% SOC imbalance introduced purposely by under-charging one of the three cells by 5% (Cell #1 in the string of 3). Thus, among the three cells in the string, Cell #1 was only at 95% SOC in the beginning of the discharge regime, while the other two were at a 100% SOC.

(2) The impact of this 5% undercharging was monitored and quantified in the subsequent tests with different protocols imposed by the control strategy variations in the RPTs.

(3) The RPTs comprise CCD regimes at the following rates: C/25, C/5, C/2 and 1C. The charge regime was conducted to maintain the 5% imbalance in the beginning of each CCD regime of a specific rate.

(4) Three different control strategies (control schemes) in the RPTs are exercised by design as follows:

Control Scheme #1. Use the same cutoff conditions as scaled up from that of the single cell (i.e. $V_{\mathbf{3S1P}\text{cutoff}} = 3 \times Vsc_{\text{cutoff}}$), where Vsc_{cutoff} is the single cell cutoff voltage (refer to Table 1). This protocol is designed to reveal the capacity of the string at full discharge under the influence of cell imbalance. The capacity delivered at different rates is determined for comparison with those of the other two schemes and that of single cell. For safety reasons, an additional safety limit was set on the single cell level at $Vsc_{\text{cutoff}} \pm 100$ mV depending upon the regime.

Control Scheme #2. Apply the test regimes within the 80%-20% SOC range. This protocol is designed to reflect a real-life operational scenario with a built in safety cushion to prevent overcharging or over discharging as the cells and string age. The 80-20% SOC range is commonly used in the field. The capacities in the CCD regimes with various rates are thus determined for comparison. The cutoff voltages were calculated from the CCD and CCC regimes at 1C rate. For example, the cutoff in the CCD regime is the voltage of the cell when discharged to 20% SOC at C/1.

Control Scheme #3. Cutoff the CCD regimes when one of the three cells in the string reaches the single cell cutoff condition. This control strategy is used in many battery management systems to protect the cells from abuse.

3. RESULTS AND DISCUSSION

3.1. Baseline performance of single cells

The ALT and SVL cells have approximately the same capacity, around 14.5 Ah at 1C as determined from the test data. It is also reflected in the results shown in Table 2, where the capacity ration (or "Q ration" in the table) shows the amount of mAh capacity corresponding to 1% SOC. The ALT cells show 154.2 mAh per 1% SOC, which would correspond to a full capacity of 15.4 Ah if all materials are used in delivering the capacity. In contrast, the SVL cells have 146.95 mAh per 1% SOC, which translates to 14.7 Ah in full capacity for the cell. In the specifications, they are rated for 13 Ah and 14 Ah, respectively.

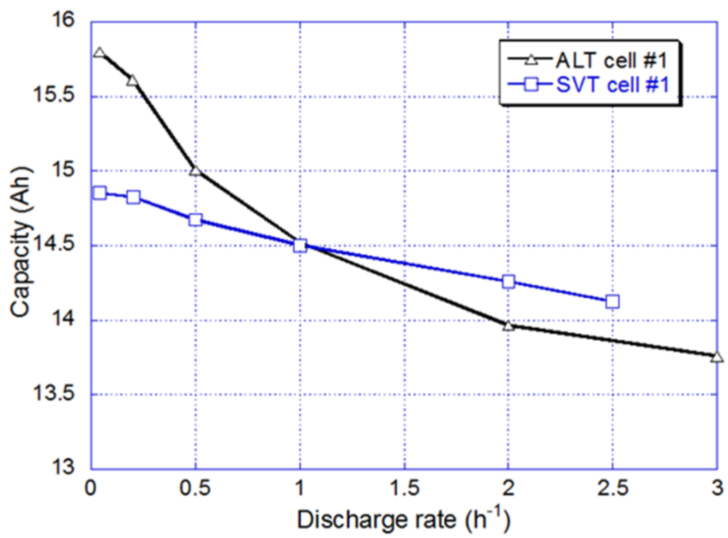

Figure 1. Comparison of rate capability as shown by the capacity versus discharge rate curves for (a) ALT and (b) SVL cell #1

Figure 1 shows the capacity variation as a function of discharge rate for the ALT and SVL cells, respectively. The results suggest that ALT cells have a lower rate capability than the SVL cells, since the capacity dependence on rate is more sensitive to rate variations as evident by the non-linearity, and slope of the curve. This is also understandable from the perspective of the materials in the electrode design. Although nLTO has been touted for its facile rate capability as an anode material, the NMC as cathode material is not a high-rate material. It is therefore likely that the NMC hampers the cell rate capability. In Table 2, the rate capability is also estimated from the capacity variation between C/2 and C/5. The simple ratio of capacity at C/2 ($Q_{C/2}$) over that at C/5 ($Q_{C/5}$) is an indication of rate capability as well. The value of the ratio $Q_{C/2}/Q_{C/5}$ is

0.967 and 0.99 for ALT and SVL cells, respectively, showcasing the difference in rate capability between the two cell designs.

The SVL cell design is intended for very high-power applications, as explained by the manufacturer and confirmed by the results of the test that revealed the high-rate capability of 0.99. The ALT cell design is intended for grid applications requiring fast charge/discharge rates, high round-trip efficiencies, long cycle life, and the ability to operate under extreme temperatures with a balanced performance between specific energy and power. The similarity in the specific energy between the two cells and the difference in the rate capability show the differences in design philosophy, objective, and potential applications.

Another useful parameter is internal ohmic resistance. The average internal ohmic resistance for the ALT cells is about 9.5 mΩ ± 10%, while SVL cells exhibit a very low ohmic resistance value of 1 mΩ ± 5%. The cell resistance variations might be a critical parameter to assess in some of the control strategies.

In addition to rate capability and resistance variations between the two cell designs the cell aging behavior would also have an impact on string performance.

Table 2. Summary of results obtained in the single cell evaluations for (a) ALT and (b) SVL cells.

(a)

	Average	Standard deviation
C/2 capacity (Ah)	14.742	0.60%
C/5 capacity (Ah)	15.242	0.74%
Rate capability	.967	0.85%
BOD RCV @ C/2 (V)	2.731	0.15%
EOD RCV @ C/2 (V)	2.062	0.85%
EOD SOC @ C/2 (%)	4.05	0.56% of SOC
BOD RCV @ C/5 (V)	2.684	0.26%
EOD RCV @ C/5 (V)	1.895	1.9%
EOD SOC @ C/5 (%)	1.44	0.3% of SOC
Resistance (mΩ)	9.51	10%
Q ration (mAh.%SOC)	154.2	0.6%
Weight (g)	400.5	0.08%
Initial OCV (V)	2.043	0.70%

(b)

	Average	Standard deviation
C/2 capacity (Ah)	13.77	1.83%
C/5 capacity (Ah)	13.96	1.71%
Rate capability	0.99	0.20%
BOD RCV @ C/2 (V)	4.09	0.06%
EOD RCV @ C/2 (V)	3.16	1.11%
EOD SOC @ C/2 (%)	2.39	0.39% of SOC
BOD RCV @ C/5 (V)	4.09	0.02%
EOD RCV @ C/5 (V)	2.98	0.66%
EOD SOC @ C/5 (%)	0.91	0.10% of SOC
Resistance (mΩ)	1.03	5.70%
Q ration (mAh.%SOC)	146.95	1.57%
Weight (g)	628.42	0.58%
Initial OCV (V)	2.565	36.1%

Figure 2(a) presents the behavior of a nominal commercial cell that consists of a graphite anode and NMC cathode [18] that follows a typical trend of aging behavior in capacity fading, whereas (b) is the cycle aging result from an ALT cell, which is also supposed to use NMC materials in the cathode, and shows that there is no fading in the initial 120 cycles of aging.

Although we do not know if the cathode materials used in this nominal commercial cell (Figure 2 bottom plot) and ALT cell (Figure 2 top plot) are similar or not, we do not anticipate such subtle difference in the cathode compositions to create a significant difference in aging behavior in the cells. Therefore, any noticeable difference in the aging behavior between the two would likely come from the anode; thus, graphite versus nLTO.

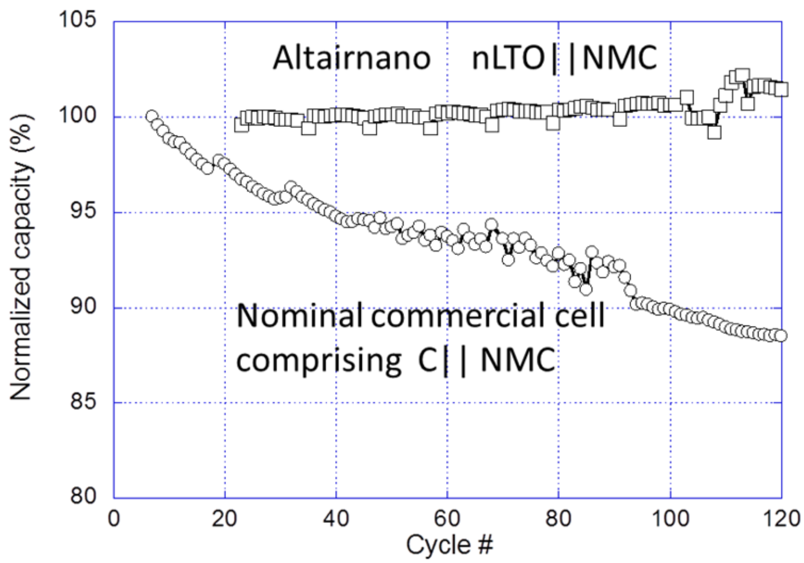

Figure 2. Capacity fade as a function of cycle number for a nominal commercial cell comprising graphite negative electrode and NMC positive electrode and ALT cell.

The capacity decrease with cycle number can be an early indicator of capacity fading with aging. This fading behavior is often attributed to the decomposition of organic electrolyte and salt in parasitic reactions at the surface of the negative electrode [9,11,14,15]. A commonly observed result of such parasitic reactions is the loss of Li inventory, where the amount of recyclable Li ions is gradually reduced in the cycle aging. The result in Figure 2 (b), top plot) suggests that this phenomenon seems to be benign in the ALT cells in contrast to the fading behavior exhibited in Figure 2 (a) bottom plot for typical commercial cells using NMC cathode and carbonaceous anode. A caution should be made here that in the ALT cell chemistry, both NMC and nLTO contain reversible Li in their compositions. The loss of Li inventory might be difficult to detect in the early stage of aging. In contrast, typical commercial cells using NMC cathode and carbonaceous anode are more vulnerable to Li inventory loss, since the Li inventory only comes from the cathode. Once lost, it is easy to detect in the aging behavior.

The SVL cells contain carbonaceous negative electrodes. This aspect leads us to believe that we would expect (although not tested) the SVL cells to follow a similar trend line in capacity fade as that shown in Figure 2 (a), bottom plot). The data for the SVL cells are not available for comparison at the writing of this report.

A unique and powerful tool to study cell aging and degradation is incremental capacity analysis [1,3,9,11,14,15]. This is a technique developed by HNEI based on prior art used in the study of electrode materials. The incremental capacity is the amount of charge (ΔQ) involved in a small interval of voltage variation (ΔV) in the path of cell reaction. In other words, the integral part of current (in a finite step of time) over a finite decimal step of voltage change in the cell ($\sum I_t \Delta t/\Delta V = \Delta Q/\Delta V$) shall represent the tendency of reaction kinetics in such a reaction at that voltage. By examining the incremental capacity curve, which exhibits the incremental capacity (ΔQ/ΔV) versus voltage for a cell, one can usually infer what the degradation might be incurring in the cell aging condition. For easy comparison, the incremental capacity is normalized to the cell's rated capacity to facilitate the comparison among cells of different capacities and designs.

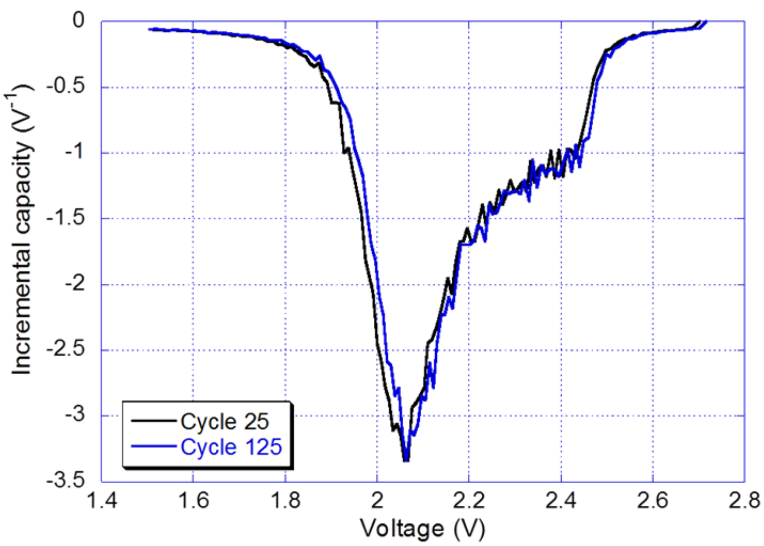

Figure 3. The incremental capacity curves for the ALT cell at cycle # 25 and 120.

Figure 3 shows the incremental capacity curve at cycle # 25 and # 120, respectively, for the ALT cell.

The similarity between the two curves shown in Figure 3 suggests that aging did not incur in any noticeable way during the initial cycle aging tests, thus the cell was not affected by the 120 cycles of aging performed.

3.2. Performance of the 3S1P strings

The influence of the control schemes on the string performance is assessed here, with a predetermined imbalance in SOC to impose sufficient imbalance in the SOC among the cells in the string. This scenario is representative of what could happen to a battery system as a result of poor quality control during manufacturing and the fidelity of cell variability data in cell selection for system assembly. For example, a potential source of imbalance could be introduced as a result of low-resolution sensors in a battery monitoring system not having the capability to accurately measure small differences in the cell voltage which could translate into a measurement error that could be several %. For example, a measurement of a few mv could be interpreted as a significant error in SOC.

Another source of imbalance among the cells could be introduced when the cells are assembled into a system. For instance, the high initial OCV spread observed in the SVT cells (±36%, Table 2) was introduced by a poor CCD handling to discharge the cells to low SOC for shipping. Before the cells are used in the assembly, they need to be carefully conditoned and fully recharged to the same SOC.

Figure 4 presents (a) the capacity retention for the ALT 3S1P string at C/2 rate under the normal CCD regime and under the three control schemes with 5% SOC imbalance in Cell #2; and, (b) the individual cell discharge curves under Control Scheme #3 at C/2. Cell #2 was the control cell with a 5% undercharge in SOC, which limits the string performance in the discharge regime.

In Figure 4(a), the green curve displays the theoretical discharge curve of a string without imbalance under controlling scheme #1, the black, blue, and red curves display the discharge curves with 5% imbalance introduced and the string operated under control schemes #1 to #3, respectively. Figure 4(b) presents the discharge curves of the 3 cells in the 3S1P assembly under control scheme #3 (red curve on Figure 4(a)).

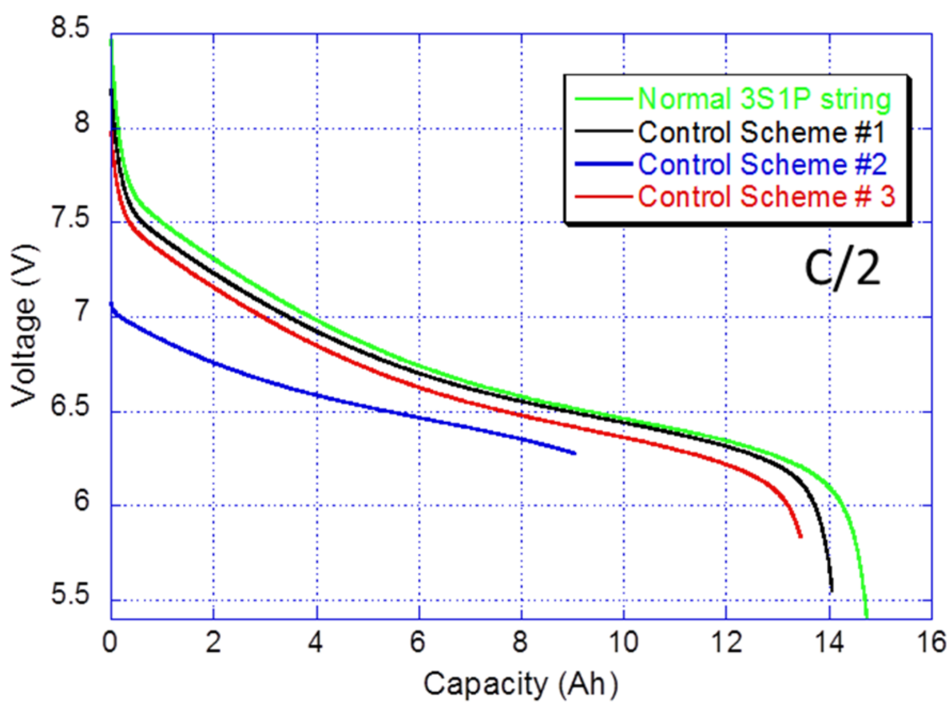

(a)

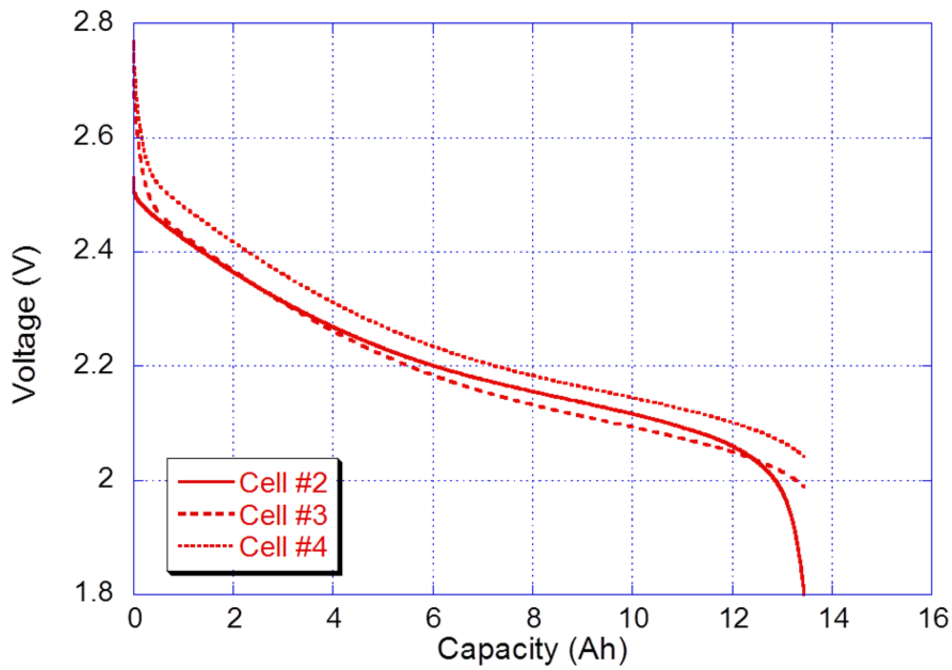

(b)

Figure 4. (a) C/2 discharge curves of the ALT 3S1P string under normal discharge conditions and under three control schemes and (b) C/2 discharge curves for the three cells in the string under control scheme #3.

Figure 5 presents similar results obtained for the experiments following the same protocols as presented in Figure 4 for the SVL 3S1P string. Similarly to the ALT string, Cell #1 (solid line in Figure 5(b)) was used in the control protocol with 5% undercharge in SOC, which limits the string performance. The color scheme is the same as the previous figure.

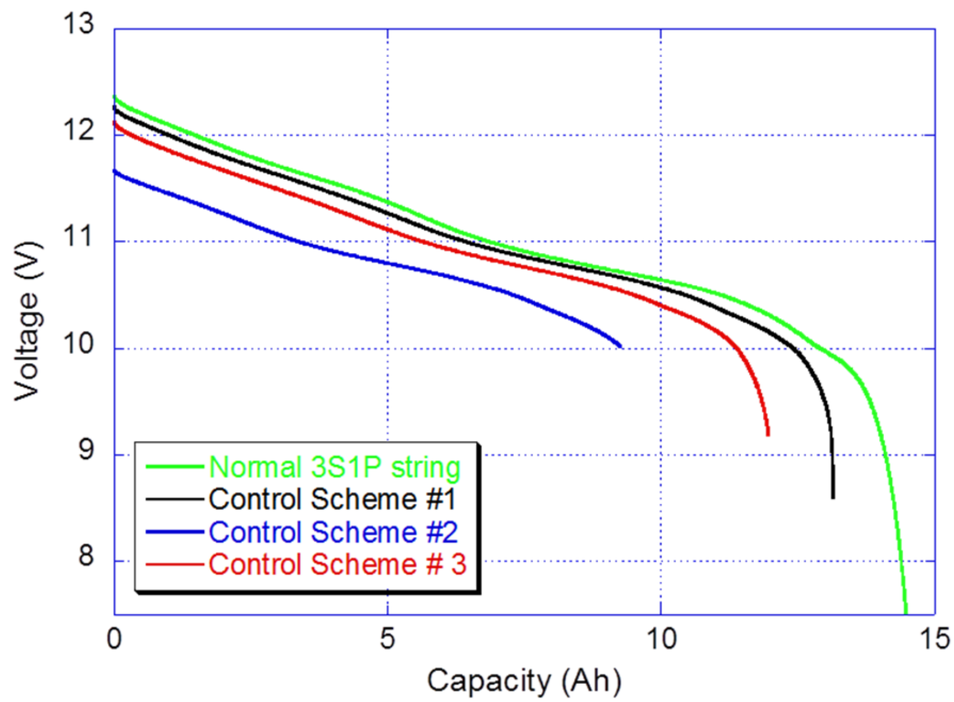

(a)

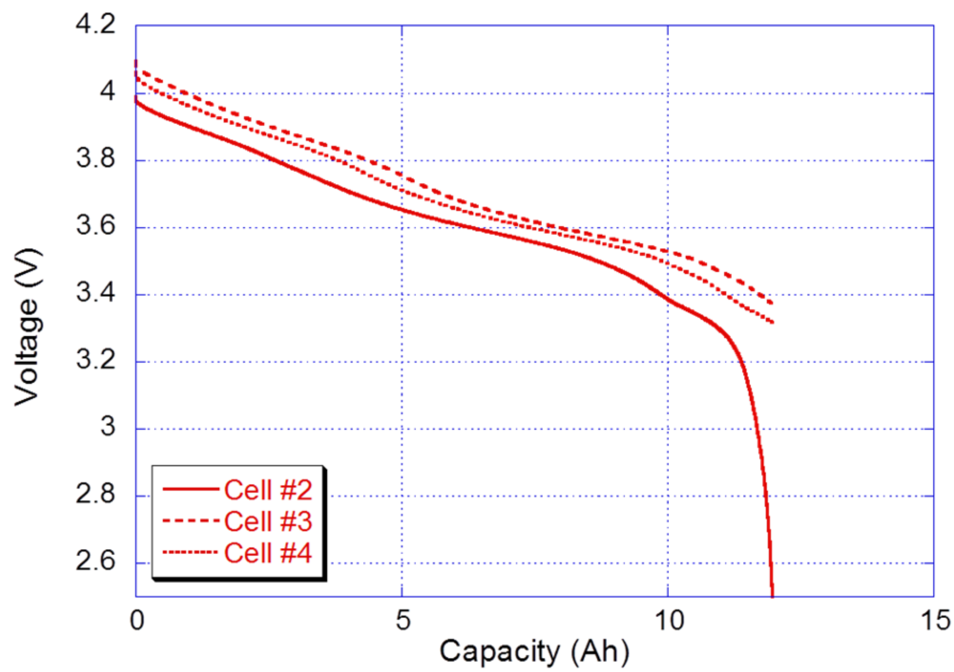

(b)

Figure 5. (a) C/2 discharge curves of the SVL 3S1P string under normal discharge conditions and under three control schemes and (b) C/2 discharge curves for the three cells in the string under control scheme #3.

Figure 6 compares the rate capability using the approach shown in Figure 4 and Figure 5 respectively, in yielding the capacity retention at four different rates (C/25, C/5, C/2 and 1C) to show the variations in the capacity retention as a function of rate with the three control schemes, as compared to that of the normal CCD regime.

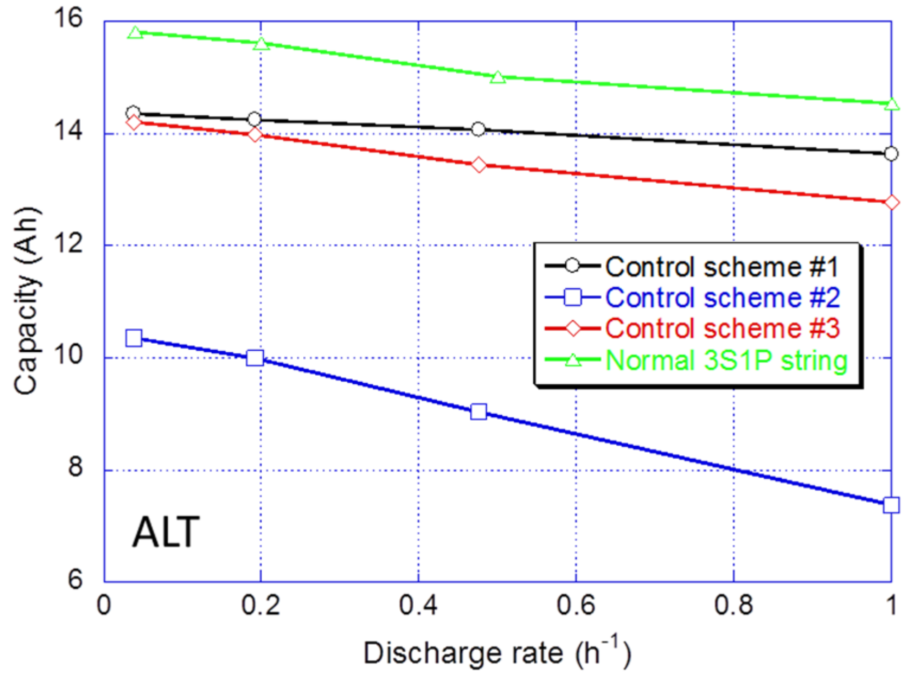

(a)

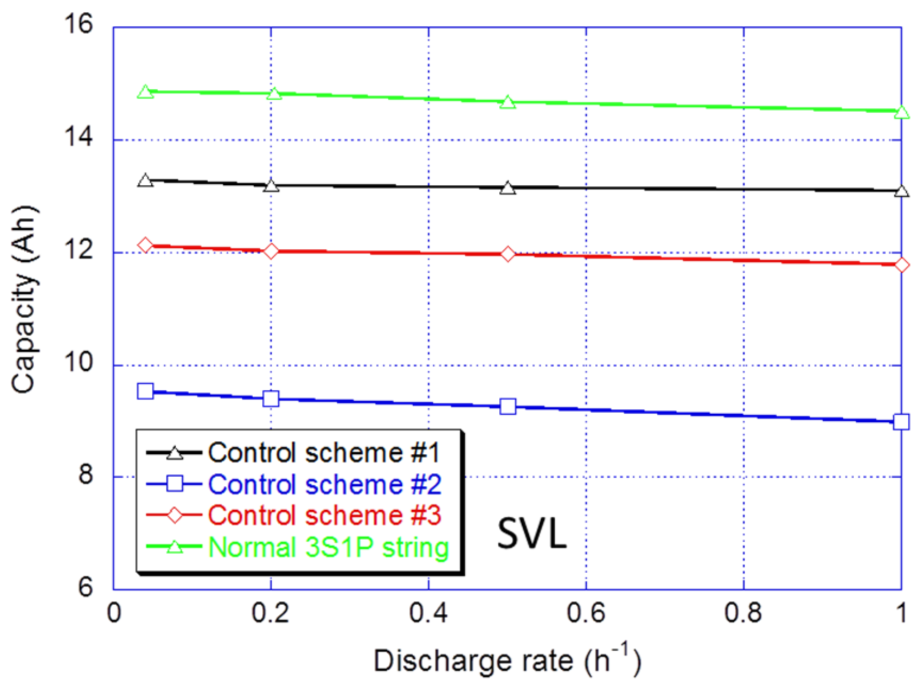

(b)

Figure 6. Comparison of rate capability between the (a) ALT and (b) SVL 3S1P string. The capacity retention as a function of discharge rate C/*n* is shown in each figure for rates of C/25, C/5, C/2 and 1C under a normal discharge regime and under the three control schemes.

Control scheme #1 which is based on the string cutoff value yields the best result among the three schemes for the ALT and SVL strings, since the capacity retention and the rate capability are the highest, (as judged from the slope of the lines – the shallower the better). However, since the strategy focuses on string level control, in both cases the cutoff condition for the string was triggered by the safety limit (charge cutoff voltage plus 0.1v) of the limiting cell (Cell #1).

Control scheme #2 results in the worst in performance of the three schemes for both ALT and SVL strings. This is understandable, since the range of the SOC was intentionally limited to 80%-20% plus the variability of the individual cells. For the ALT cells, not only the charge retention for all rates is significantly lower, but also the rate capability (the slope of the curve is the highest) is lower than those of the other two schemes. For the SVL cells, the charge retention is also greatly reduced by the limited SOC range. The rate capability (slope of the curve) was not affected very much by the scheme, as a benefit of the high-power design.

Control scheme #3 is based on the single cell cutoff value and is more conservative than control scheme #1. Also the capacity retention and rate capability are lower than those used in control scheme #1. The conservative approach presented in this strategy might result in better durability than control scheme #1, since adverse abuse conditions are minimized in the scheme.

In Figure 6(a), for the ALT design, the difference in capacity between control schemes #1 and #3 starts off relatively small; but as rate increases, their differences increase as well. The rate capability under control scheme #1 is better (i.e. the slope of the curve is less steep) than under control scheme #3 and the single cell (or string without the predetermined imbalance).

In Figure 6(b), for the SVL design, the difference in capacity between control schemes #1 and #3 is less dependent upon the rate. The two curves are essentially parallel over the CCD test regimes.

4. CONCLUSION

The performance of two types of cells provided by Altairnano and SAFT in a 3S1P string configuration was evaluated. Reference performance tests were used to characterize the baseline performance characteristics of the ALT and SVL cells. The test results show the design differences between the two types of cells. The ALT design (nLTO//NMC) optimizes high energy and power, while minimizing capacity fade. The SVL design optimizes cell performance for high-power applications.

A 3S1P string consisting of each type of cell was tested to derive the string performance characteristics utilizing three different control schemes. The observed differences among the three control schemes show sensitivity to the cell imbalance and test protocols. The cell imbalance was predetermined by design with one of the three cells intentionally under-charged by 5% (in SOC). By combining the cell imbalance and control scheme, the performance of the strings can be compromised.

Although the tests are quite preliminary, the results are useful to illustrate the points regarding the impacts on string performance attributed to cell design, cell imbalance in a string configuration, and the test protocols as implemented by control schemes.

The results obtained from the analysis of three control schemes would be useful in matching the cell technology and design to a given application in electrical energy storage for grid and distributed energy storage systems.

For example, high-power performance and fast charge/discharge rates are desired for frequency and voltage regulation, where low impedance in the cell and spontaneous response to improve power factor is a critical consideration. On the other hand, to support peak shaving and ancillary services like spin reserve, a more balanced energy-power design might be more suitable to achieve the goals.

5. REFERENCES

1. Final report for Task “Cell Testing” funded by the US Department of Energy, Project “Hawai‘i Energy Sustainability Program.” Contract No. DE-EE0003507.
2. M. Dubarry, V. Svoboda, R. Hwu, B.Y. Liaw. “Capacity and power fading mechanism identification from a commercial cell evaluation.” *J. Power Sources* 165 (2007) 566.
3. M. Dubarry, V. Svoboda, R. Hwu, B.Y. Liaw. “Capacity loss in rechargeable lithium cells during cycle life testing: The importance of determining state-of-charge.” *J. Power Sources* 174 (2007) 1121.
4. M. Dubarry, V. Svoboda, R. Hwu, B.Y. Liaw. “A roadmap to understand battery performance in electric and hybrid vehicle operation.” *J. Power Sources* 174 (2007) 366.
5. B.Y. Liaw, G. Nagasubramanian, R.G. Jungst, D.H. Doughty. “Modeling of lithium ion cells.” *Solid State Ionics* 175 (2004) 835.
6. B.Y. Liaw, R.G. Jungst, G. Nagasubramanian, H.L. Case, D.H. Doughty. “Modeling capacity fade in lithium-ion cells.” *J. Power Sources* 140 (2005) 157.
7. M. Dubarry, B.Y. Liaw. “Development of a universal modeling tool for rechargeable lithium batteries.” *J. Power Sources* 174 (2007) 856.
8. M. Dubarry, N. Vuillaume, B.Y. Liaw. “From single cell model to battery pack simulation for Li-ion batteries.” *J. Power Sources* 186 (2009) 500.
9. M. Dubarry, B.Y. Liaw. “Identify capacity fading mechanism in a commercial $LiFePO_4$ Cell.” *J. Power Sources* 194 (2009) 541.
10. M. Dubarry, N. Vuillaume, B.Y. Liaw. “Origins and accommodation of cell variations in Li-ion battery pack modeling.” *Int. J. Energy Res.* 34 (2010) 216.
11. M. Dubarry, B.Y. Liaw, M-S. Chen, S-S. Chyan, K-C. Han, W-T. Sie, S-H. Wu. “Identifying battery aging mechanisms in large format Li ion cells.” *J. Power Sources* 196 (2011) 3420.
12. K.L. Gering, S.V. Sazhin, D.K. Jamison, C.J. Michelbacher, B.Y. Liaw, M. Dubarry, M. Cugnet. “Investigation of path dependence in commercial lithium-ion cells chosen for plug-in hybrid vehicle duty cycle protocols.” *J. Power Sources* 196 (2011) 3395.
13. M. Dubarry, C. Truchot, M. Cugnet, B.Y. Liaw, K.L. Gering, S.V. Sazhin, D.K. Jamison, C.J. Michelbacher. “Evaluation of commercial lithium-ion cells based on composite positive electrode for plug-in hybrid electric vehicle (PHEV) applications. Part I. Initial characterizations.” *J. Power Sources* 196 (2011) 10328.
14. M. Dubarry, C. Truchot, B.Y. Liaw, K.L. Gering, S.V. Sazhin, D.K. Jamison, C.J. Michelbacher. “Evaluation of commercial lithium-ion cells based on composite positive electrode for plug-in hybrid electric vehicle (PHEV) applications. Part II. Degradation mechanism under 2C cycle aging.” *J. Power Sources* 196 (2011) 10336.
15. M. Dubarry, C. Truchot, B.Y. Liaw. “Synthesize battery degradation modes via a diagnostic and prognostic model.” *J. Power Sources* 219 (2012) 204.
16. M. Dubarry, C. Truchot, B.Y. Liaw, K. Gering, S. Sazhin, D. Jamison, C. Michelbacher. “Evaluation of commercial lithium-ion cells based on composite positive electrode for plug-in hybrid electric vehicle applications. Part III. Aging through temperature excursions,” submitted to *J. Electrochem. Soc*. (manuscript in revision)
17. B.Y. Liaw, M. Dubarry. “A roadmap to understand battery performance in electric and hybrid vehicle operation.” in *Electric and Hybrid Vehicles. Power Sources, Models,*

Sustainability, Infrastructure and the Market, G. Pistoia, ed., Elsevier Science BV, Amsterdam, Netherlands, 2010. Chapter 15, pp 375–403.
18. Unpublished results from another testing project not within the scope of this work.
19. T. Ohzuku, A. Ueda, N. Yamamota. “Zero-strain insertion material of $Li[Li_{1/3}Ti_{5/3}]O_4$ for rechargeable lithium cells.” *J. Electrochem. Soc*. 142 (1995) 1431.
20. K. Zaghib, M. Simoneau, M. Armand, M. Gauthier. “Electrochemical study of $Li_4Ti_5O_{12}$ as negative electrode for Li-ion polymer rechargeable batteries.” *J. Power Sources* 81–82 (1999) 300.